Fusion Engineering and Design 215 (2025) 115009

Contents lists available at ScienceDirect

Fusion Engineering and Design

journal homepage: www.elsevier.com/locate/fusengdes

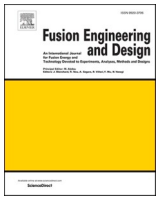

Scoping analysis of the influence of initial temperature on D/T-air ignition risk in a vacuum chamber

Jean-François Ciparisse *, Danilo Nicola Dongiovanni

NUC-TEN department, ENEA, CR. Frascati, Via Enrico Fermi, 45, Frascati, Rome 00044, Italy

ARTICLE INFO

Keywords:
LOVA
Detailed mechanism
Large eddy simulation

ABSTRACT

DEMO (Demonstration Fusion Power Reactor) is a new nuclear power plant aiming at demonstrating that electricity can be produced from fusion reactions. In such a facility, all potential safety issues must be assessed and addressed in order to minimize the risk of accidents. Among those, fires and explosions represent some of the main threats during plant operation. One of the reference accident events is the LOVA (Loss of Vacuum Accident) in the DEMO Tokamak due to the postulated breach of one of the lines Vacuum Vessel (VV) connected volumes. The accident transient sequence considers the air entering the VV, initially in vacuum condition, to mix with the deuterium-tritium therein contained and the possible flame ignition in case of heat source. When simulating such a complex phenomenology, several initial and boundary conditions, as well as input parameters representative for the considered safety case shall be defined.

To this end, as a preliminary analysis, a LOVA in a simple spherical tank, containing a hot equimolar mixture of deuterium and tritium, was considered. The volume of this vessel was taken equal to 1 m^3 and an air ingress through a pipe whose axis is directed radially with respect to the tank was simulated numerically by means of open-source software OpenFOAM to simulate the air expansion in the vessel as well as the chemical reactions that may occur. Three initial temperatures of the D/T mixture were considered as conditions that may occur: 400 K, 900 K and 1300 K, based on the temperature range that is expected to exist on the plasma-facing components and in the vessel during operation and when decay heat is produced.

On the basis of the observed fields of temperature, combustion intensity and water mass fraction, the risk of ignition was assessed for each considered case.

1. Introduction

In the general framework of green transition toward decarbonized energy sources, fusion plants are believed to play a key role in the decades to come, as they promise to produce continuously power with no greenhouse gases emissions and with a very little amount of radioactive waste, compared to traditional fission plants. As improvements are made in the myriad of fields that are involved in fusion technology development (neutronics, plasma physics, superconductivity, diagnostics, etc.), safety analyses concerning plants to be built are necessary to assess all possible incident and accident scenarios during the life of fusion power plants. As in every industrial facility, fires and explosions due to reactions of air and combustible materials are one of the major concerns.

In Tokamaks, the vacuum vessel contains hydrogen isotopes (deuterium and tritium), as well as metallic dust produced by first wall erosion due to plasma disruptions and operation [1,2]. Substantial inventories of hydrogen isotopes will be present in parts of the DEMO plant owing to the higher throughput of deuterium and tritium fuels. DEMO In-VV inventory for tritium is assumed in the 2–4 kg range [3]. A further inventory of up to 1350 g of hydrogen isotopes segregated in plasma facing surfaces [4] can also be added.

In case of a Loss Of Vacuum Accident (LOVA) [5], there is a risk for the D/T-air mixture to ignite due to high initial temperature of hydrogen or because of hot spots and sparks on walls and eventually trigger the explosion of a dust cloud, as stated in [1,5]. As a consequence of the latter event, vessel failure and activated dust release outside the reactor may occur.

Current safety studies on validated codes (e.g. MELCOR code for severe accident simulation [6]) rely on time-averaged reaction rates for the leading reactions (e.g. $H_2 + ½\ O_2$ -> H_2O) and 0-D relative H_2, O_2, steam species concentrations to determine whether the mixture is flammable. The complex phenomenology occurring during accident

* Corresponding author.
E-mail address: jeanfrancois.ciparisse@enea.it (J.-F. Ciparisse).

https://doi.org/10.1016/j.fusengdes.2025.115009
Received 28 November 2024; Received in revised form 17 February 2025; Accepted 26 March 2025
Available online 1 April 2025

transient, though requires both a better definition of chemical reaction chain and a 3D domain modelling enabling the investigation of local effects (both thermal exchange and fluid dynamic) impact on transient evolution so to correctly assess whether DEMO is kept within safe domain during the whole transient. A 3D-CFD modelling approach has been exploited in some literature studies [7–10] in order to overcome the limitations of 0D codes.

Present work proposes numerical simulations of a LOVA in a spherical vessel were carried out with OpenFOAM software including a detailed reaction mechanism (9 species and 21 reactions) as well as large eddy simulation (LES) turbulent modelling. DEMO was taken as the reference case study and the D/T initial content was scaled to the sphere's volume accordingly. As it is crucial to correctly predict whether or not an ignition occurs, an initial study of the reaction rate of hydrogen/air mixture was carried out by means of an array of simulations performed with OpenFOAM at several temperatures in the range 700K-1300 K for five detailed mechanisms. This activity led to the determination of the kinetic scheme that better predicts the autoignition temperature of a hydrogen/air stoichiometric mixture (average value of 832 K, as reported in [11]). Afterwards, three simulations of a LOVA in the spherical vessel were performed at an initial temperature of 400 K, 900 K and 1300 K. The considered physical time was 0.03 s. For each case, the occurrence of a flame formation was assessed.

2. Physical models and numerical settings

2.1. Computational domain

The case study considered is a sub-atmospheric spherical vessel, having a volume of 1 m^3 (0.61 m radius) connected to environment at STP through a straight pipe whose diameter is 0.003 m, as shown in Fig. 1:

2.2. Models

The problem studied involves several phenomena: turbulent supersonic flow, multicomponent diffusion, chemical reactions and heat release.

2.2.1. Conservation equations

The general fluid-dynamic problem of a highly compressible reacting flow simulated by means of large eddy simulation (LES) approach can be mathematically formalized as:

$$\frac{\partial}{\partial t}\iiint \vec{U}dV+\sum_{i=1}^{i=3}\iint\left(\vec{F}_i^C-\vec{F}_i^D\right)n_i dA=\iiint \vec{S}dV \tag{1}$$

where $\vec{U}$ is the vector of conservative variables in generic control volume V. Eq. (1) establishes the conservation in V of the variables that describe the whole phenomenon: mass, momentum, energy and species mass fraction. The time derivative of the volume integral on V of a given quantity is expressed as the balance of fluxes of the same quantity on the boundaries of V plus a source term. $\vec{F}_i^C$ and $\vec{F}_i^D$ are, respectively, the i-th component of convective flux vector and diffusive flux vector through the control volume surface ∂V. n_i is the i-th component of the outward-pointing unit vector normal to ∂V and $\vec{S}$ is the vector of source terms [12]. Given a generic quantity φ, $\overline{\varphi}$ is its spatially filtered value whereas $\widetilde{\varphi}=\frac{\overline{\rho\varphi}}{\overline{\rho}}$ is its Favre-averaged value. In LES approach, the flow is directly resolved at level of the cells composing the grid, whereas the finest structures (small eddies) that are present at spatial scales smaller than the ones of the mesh are modelled.

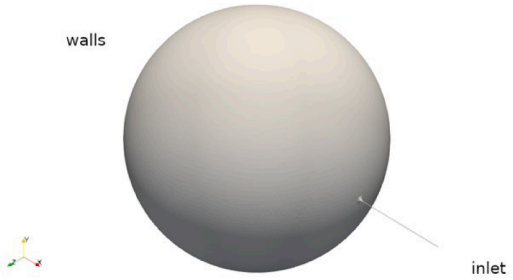

Fig. 1. Geometry.

The above-mentioned terms that appear in Eq. (1) are expressed as follows:

$$\vec{U}=\begin{Bmatrix}\overline{\rho}\\ \overline{\rho}\widetilde{u}_i\\ \overline{\rho}\widetilde{E}\\ \overline{\rho}\widetilde{Y}_k\end{Bmatrix},\ \vec{F}_i^C=\begin{Bmatrix}\overline{\rho}\widetilde{u}_i\\ \overline{\rho}\widetilde{u}_i\widetilde{u}_j+\overline{p}\delta_{ij}\\ \overline{\rho}\widetilde{u}_i\widetilde{H}\\ \overline{\rho}\widetilde{u}_i\widetilde{Y}_k\end{Bmatrix},$$

$$\vec{F}_i^D=\begin{Bmatrix}0\\ \overline{\sigma}_{ij}+\sigma_{ij}^{sgs}\\ \overline{\sigma_{ik}u_k}-\overline{q}_i-q_i^{sgs}\\ \overline{j}_i+j_i^{sgs}\end{Bmatrix},\ \vec{S}=\begin{Bmatrix}0\\ 0\\ 0\\ \overline{\dot{\omega}_k}\end{Bmatrix} \tag{2}$$

where ρ is the density, u_i is the i-th component of the velocity vector, δ_{ij} is the Kronecker symbol, p is the pressure, $E=\sum_{k=1}^{k=N}Y_k h_k+\frac{u_i^2}{2}-\frac{p}{\rho}$ is the total internal energy, H is the total enthalpy, Y_k is the k-th species mass fraction, h_k is its enthalpy and N is the number of species. The diffusion terms for momentum, energy and species mass fraction appearing in $\vec{F}_i^D$ depend linearly on the space derivatives of velocity components, temperature and mass fraction and are modelled respectively as:

$$\sigma_{ij}=\mu\left(\frac{\partial u_i}{\partial x_j}+\frac{\partial u_j}{\partial x_i}\right)-\frac{2}{3}\mu\frac{\partial u_k}{\partial x_k}\delta_{ij} \tag{3}$$

$$q_i=-\lambda\frac{\partial T}{\partial x_i}-\sum_{k=1}^{k=N}\rho D_k h_k\frac{\partial Y_k}{\partial x_i} \tag{4}$$

$$j_i=-\rho D_{km}\frac{\partial Y_k}{\partial x_i} \tag{5}$$

where the molecular transport properties of the mixture (μ, λ and D_{km}) are calculated from the properties of each of the N species according to Wilke's mixing rule [13]:

$$\mu=\sum_{k=1}^{k=N}\frac{\mu_k}{1+\frac{1}{Y_k}\sum_{l=1,\ l\neq l}^{l=N}Y_k\varphi_{kl}} \tag{6}$$

$$\varphi_{kl}=\frac{\left[1+\sqrt{\frac{\mu_k}{\mu_l}}\cdot\sqrt[4]{\frac{M_l}{M_k}}\right]^2}{\frac{4}{\sqrt{2}}\cdot\sqrt{1+\frac{M_k}{M_l}}} \tag{7}$$

where M_k and M_l are the molar masses of k-th and l-th species.

For each species, the molecular transport properties depend on temperature. To consider this effect, Sutherland's formula was applied to viscosity:

$$\mu_k=\frac{A_k T^{3/2}}{T+T_k} \tag{8}$$

where A_k and T_k are constants specific to each species. λ_k and D_k are calculated as:

$$\lambda_k = \frac{C_{p,k}\mu_k}{Pr} \tag{9}$$

$$D_k = \frac{\mu_k}{\rho Sc} \tag{10}$$

where C_{pk} is the constant pressure specific heat for k-th species, and Pr is the Prandtl number and Sc is the Schmidt number. Pr and Sc are assumed to be constant with temperature and equal for all species. Their values are, respectively, 0.7 and 1. Eqs. (8)–(10) account for the increase with temperature of molecular diffusion.

Constant pressure specific heats are calculated in function of temperature as two-range polynomials [14]:

$$C_{p,k} = a_{0,k} + a_{1,k}T + a_{2,k}T^2 + a_{3,k}T^3 + a_{4,k}T^4 \tag{11}$$

where all constants, specific to each species, are obtained by fitting experimental data.

Mixture density is calculated with perfect gas law:

$$\rho = \frac{p}{TR_u \sum_{k=1}^{k=N} \frac{Y_k}{M_k}} \tag{12}$$

where $R_u = 8.314\ J/(molK)$ is the universal gas constant and mixture constant pressure specific heat is given by:

$$C_{p,m} = \sum_{k=1}^{k=N} C_{p,k} Y_k \tag{13}$$

The additional subgrid diffusive terms that appear after LES filtering in $\overrightarrow{F}_i^D$ depend on Favre-averaged and filtered components of velocity, temperature and species mass fraction and are modelled as follows:

$$\sigma_{ij}^{sgs} = -\left(\overline{\rho u_i u_j} - \overline{\rho}\widetilde{u}_i\widetilde{u}_j\right)$$

$$= \frac{1}{3}\sigma_{kk}^{sgs} - 2\overline{\rho}\upsilon_t\left(\widetilde{S}_{ij} - \frac{1}{3}\widetilde{S}_{kk}\delta_{ij}\right) \tag{14}$$

$$\widetilde{S}_{ij} = \frac{1}{2}\left(\frac{\partial\widetilde{u}_i}{\partial x_j} + \frac{\partial\widetilde{u}_j}{\partial i}\right) \tag{15}$$

$$q_i^{sgs} = \overline{\rho u_i H} - \overline{\rho}\widetilde{u}_i\widetilde{H} = -\frac{\overline{\rho}\upsilon_t C_{p,m}}{Pr_t^{sgs}}\frac{\partial\widetilde{T}}{\partial x_i} \tag{16}$$

$$j_i^{sgs} = -\left(\overline{\rho u_i Y_k} - \overline{\rho}\widetilde{u}_i\widetilde{Y}_k\right) = -\frac{\overline{\rho}\nu_t}{Sc_t^{sgs}}\frac{\partial\widetilde{Y}_k}{\partial x_i} \tag{17}$$

where $Pr_t^{sgs} = 0.85$ and $Sc_t^{sgs} = 0.7$. $\sigma_{ij}^{sgs}, q_i^{sgs}$ and j_i^{sgs} are the subgrid diffusive fluxes of, respectively, momentum, energy and species mass fraction.

The LES model that has been adopted is WALE (Wall-Adapting Local Eddy-viscosity) and the turbulent kinematic viscosity, υ_t, is related to the subgrid length and to the velocity spatial derivatives as follows [15]:

$$\upsilon_t = (C_w\Delta)^2\frac{\left(s_{ij}^d s_{ij}^d\right)^{3/2}}{\left(\widetilde{S}_{ij}\widetilde{S}_{ij}\right)^{5/2} + \left(s_{ij}^d s_{ij}^d\right)^{5/4}} \tag{18}$$

$$s_{ij}^d = \frac{1}{2}\left(\overline{g}_{ij}^{\,2} + \overline{g}_{ji}^{\,2}\right) - \frac{1}{3}\overline{g}_{kk}^{\,2}\delta_{ij} \tag{19}$$

$$\overline{g}_{ij}^{\,2} = \overline{g}_{ik}\overline{g}_{kj} = \frac{\partial\widetilde{u}_i}{\partial x_k}\frac{\partial\widetilde{u}_k}{\partial x_j} \tag{20}$$

where $C_w = 0.325$ and Δ is the subgrid characteristic length (taken equal to the local size of the cells).

Finally, $\overline{\dot{\omega}_k}$ is determined by the Arrhenius's law, as explained in paragraph 2.2.2.

2.2.2. Species and detailed mechanism

As this study is focused on the assessment of the ignition risk of D/T mixture, a detailed combustion mechanism involving the 9 main species that are expected to be present (O_2, H_2, OH, O, H, H_2O, HO_2, H_2O_2 and N_2) was considered. As it will be shown in paragraph 3, temperature does not exceed 1300 K (case 3), except during the very first moments of the simulations. Therefore, N_2 is assumed to be an inert species and no compounds containing nitrogen are taken into account in the kinetic mechanism. Instead of considering, for the species containing hydrogen (for example OH), the two isotopes (deuterium and tritium) and considering different species (i.e. OD and OT instead of OH), a fictious hydrogen isotope, having intermediate molar mass (2.5 g/mol, as the mixture of D/T is equimolar and the molar masses are respectively 2 and 3 g/mol) was chosen as a replacement. This greatly reduces the computational cost.

As the molar mass affects properties as molecular diffusion and thermal conductivity, these properties were changed consequently for the species containing hydrogen with respect to the default values when the hydrogen isotope is protium.

The reaction rate of a single step is related to the Arrhenius' equation:

$$k = AT^b\exp\left(\frac{-T_A}{T}\right) \tag{21}$$

where A is the collisional frequency, T is the absolute temperature, b is the temperature exponent and T_A is the activation temperature of the step considered. As explained previously, a preliminary assessment of the capability of several mechanisms to predict the ignition of a hydrogen mixture in air was carried out. As each mechanism is tailored for particular conditions of interest (equivalence ratio, initial temperature, pressure), the above-mentioned constants greatly differ from one mechanism to another.

In order to avoid incorrect prediction of the ignition risk of a mixture of hydrogen and air, five detailed mechanisms ([16–20]) were tested to determine the one that ensures the best agreement of the ignition temperature with the one reported in literature (832 K).

To this end, a set of simulations was carried out in a cubic test domain (10 × 10 × 10 cm) whose boundaries are walls. Uniform temperature was imposed on them and set to five different values: 700, 750, 800, 850 and 900 K. The domain contains a stoichiometric mixture of hydrogen and air initially at room conditions (1 atm and 300 K).

For each one of the 25 combinations of mechanism and temperature (5 × 5), the peak temperature was taken as the observable quantity to establish whether combustion occurs or not. A minimum rise of 500 K above the initial 300 K was considered to be the threshold. For all simulations, the physical duration was set to 2 s.

The computational domain has 1000,000 hexahedral cells with wall mesh refining, as shown in Fig. 2:

Finally, the mechanism that gave the best result (850 K) was the one proposed by the University of San Diego [16].

Table 1 reports the 21 elementary steps involving the 9 species, as well as the values of the constants in the default units for OpenFOAM:

2.2.3. Boundary and initial conditions

Taking as a reference DEMO fusion plant scaled to considered geometry: i) a 50/50% molar D/T mixture fills the domain; the initial mass of gas is 1.2 g scaled from the full inventory of D/T mixture in the vacuum vessel (in the order of 4.5 kg); ii)under the assumption of thermal equilibrium between chamber walls and D/T mixture, the considered range of temperatures is varied between 400 K and 1300 K as reported in [21,3]. The following initial conditions were therefore imposed:

1. Case 1: T = 400 K, p = 490 Pa
2. Case 2: T = 900 K, p = 1100 Pa

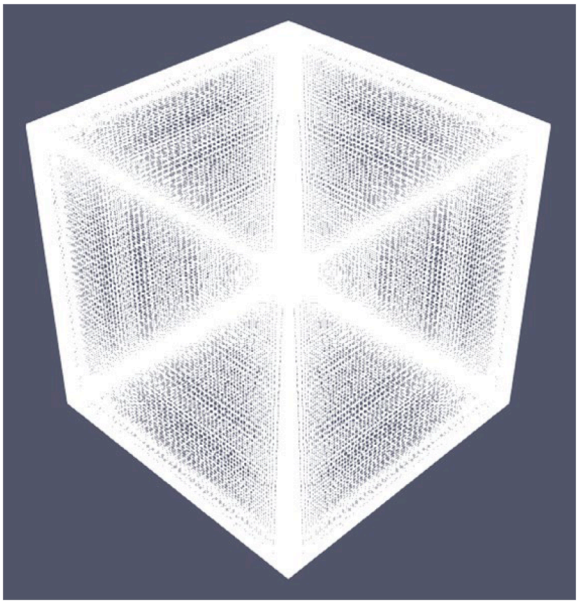

Fig. 2. Test domain mesh.

Table 1
USCD hydrogen-air detailed combustion mechanism.

Reaction		A*	b	Ta (K)
$H + O_2 \leftrightarrow OH + O$		3.52E+13	−0.7	8590.3
$H_2 + O \leftrightarrow OH + H$		50.6	2.67	3165.7
$H_2 + OH \leftrightarrow H_2O + H$		1.17E+06	1.3	1829.44
$H_2O + O \leftrightarrow 2OH$		7.06E-03	3.84	6431.3
$2H + M \leftrightarrow H_2 + M$[a]		1.30E+12	−1	0
$H + OH + M \leftrightarrow H_2O + M$[a]		4.00E+16	−2	0
$2O + M \leftrightarrow O_2 + M$[a]		6.17E+09	−0.5	0
$H + O + M \leftrightarrow OH + M$[a]		4.71E+12	−1	0
$O + OH + M \leftrightarrow HO_2 + M$[a]		8.30E+08	0	0
$H + O_2 + M \leftrightarrow HO_2 + M$[b]	k_0	5.75E+13	−1.4	0
	k_∞	4.65E+09	0.44	0
$HO_2 + H \leftrightarrow 2OH$		7.08E+10	0	147.94
$HO_2 + H \leftrightarrow H_2 + O_2$		1.66E+10	0	413.75
$HO_2 + H \leftrightarrow H_2O + O$		3.10E+10	0	866
$HO_2 + O \leftrightarrow OH + O_2$		2.00E+10	0	0
$HO_2 + OH \leftrightarrow H_2O + O_2$		2.89E+10	0	−250.18
$2OH + M \leftrightarrow H_2O_2 + M$[c]	k_0	2.30E+12	−0.9	−855.42
	k_∞	7.40E+10	−0.37	0
$2HO_2 \leftrightarrow H_2O_2 + O_2$		3.02E+09	0	697.6
$H_2O_2 + H \leftrightarrow HO_2 + H_2$		4.79E+10	0	4005.3
$H_2O_2 + H \leftrightarrow H_2O + OH$		1.00E+10	0	1804.44
$H_2O_2 + OH \leftrightarrow H_2O + HO_2$		7.08E+09	0	721.67
$H_2O_2 + O \leftrightarrow HO_2 + OH$		9630	2	2008.7

* units are kmol, m^3 and s
[a] Chaperon efficiencies are 2.5 for H_2, 16 for H_2O and 1 for all other species. Troe falloff with Fc = 0.5.
[b] Chaperon efficiencies are 2.5 for H_2, 12 for H_2O and 1 for all other species.
[c] Chaperon efficiencies are 2.5 for H_2, 6 for H_2O and 1 for all other species: Fc = 0.265exp(-T/(94 K)) + 0.735exp(-T/(1756 K)) + exp((−5182 K)/T).

3. Case 3: T = 1300 K, p = 1592 Pa

The following boundary conditions were imposed:

- Walls: adiabatic because of the very short transient duration, no-slip
- Inlet: air, total temperature of 300 K, total pressure ramping from initial pressure to 1 atm in 0.001 s.

A gradual variation of pressure takes into account the progressive formation of the breach, whose duration is affected by a number of factors. The estimation of the order of magnitude of this transient time was done by considering that the ingress of air takes place through a circular Cross-scored rupture disk staying at the inlet, notwithstanding that its layout, shown in Fig. 3 [22], does not correspond to the one of a real breach:

The inlet total pressure rise time was assumed to coincide with the disk opening time, whose expression is reported in [22]:

$$t = 0.93\left(\frac{\rho\tau l}{\Delta p}\right)^{1/2} \tag{22}$$

where ρ is the thickness of the sheet of metal that breaks, τ is its thickness, l is the length of a square whose surface is equal to the one of the rupture disk and Δp is the pressure difference across the latter. In our case, the cross section to be taken into account is the one relative to the pipe diameter. Therefore, l is given by:

$$l = r\sqrt{\pi} \tag{23}$$

where r is the radius of the pipe. Eq. (22) then becomes:

$$t = 0.93\left(\frac{\rho\tau r\sqrt{\pi}}{\Delta p}\right)^{1/2} \tag{24}$$

Assuming that $\rho = 7800\ \frac{kg}{m^3}$, $\tau = 0.002\ m$, $r = 0.0015\ m$ and $\Delta p = 10^5\ Pa$, $t = 6{\cdot}10^{-4}\ s$. A value of 1 ms was then chosen as it is sufficiently small not to affect the overall results of the simulation that lasts 0.03 s, while being sufficiently long to reproduce a real failure of the vacuum containment.

2.2.4. Mesh

A polyhedral mesh with wall refinement was used. A convergence study was performed on three grids with increasing refinement level: a coarse mesh with about 300,000 cells, a medium mesh with 750,000 cells and a fine mesh with 1500,000 cells. In all cases, wall functions were used to avoid an excessively fine grid at walls. The convergence criterion used in this study was the peak mass fraction of water during the simulation. It was found that coarse mesh leads to an underestimation of water production with respect to the results of the other two, which are in good agreement. Finally, the fine mesh (1500,000 cells) was adopted.

3. Results

For the three cases, Mach number, temperature, combustion intensity and H_2O mass fraction fields are shown at 0.002 s, 0.01 s and 0.03 s on xz plane. Figs. 4–6 show, respectively, the results for Cases 1, 2 and 3. Fig. 7 shows the plots versus time of the comparisons between the three cases of the maximum values of the quantities mentioned above that are found in the whole domain.

3.1. Case 1

As air penetrates through the pipe in the vacuum chamber, it expands and reaches a constant Mach number of 2.9 in a bubble located at the connection between the duct and the sphere, inducing a compression of the D/T mixture and a temporary temperature raise up to 1900 K at the end of the total pressure ramp at the inlet (0.001 s). This compressive effect locally and temporarily ignites the air/hydrogen mixture that

Fig. 3. Cross-scored rupture disk.

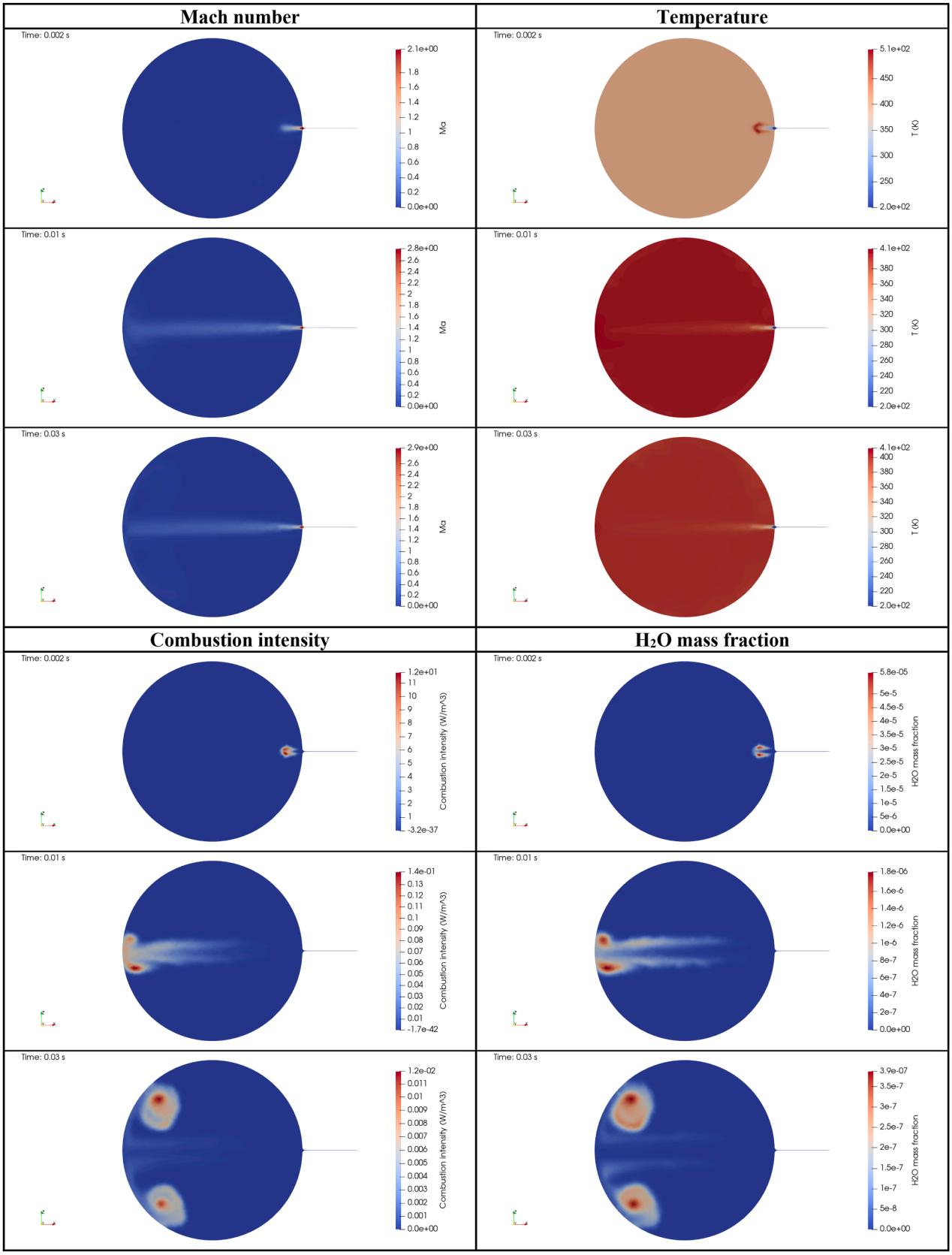

Fig. 4. Fields vs time for Case 1.

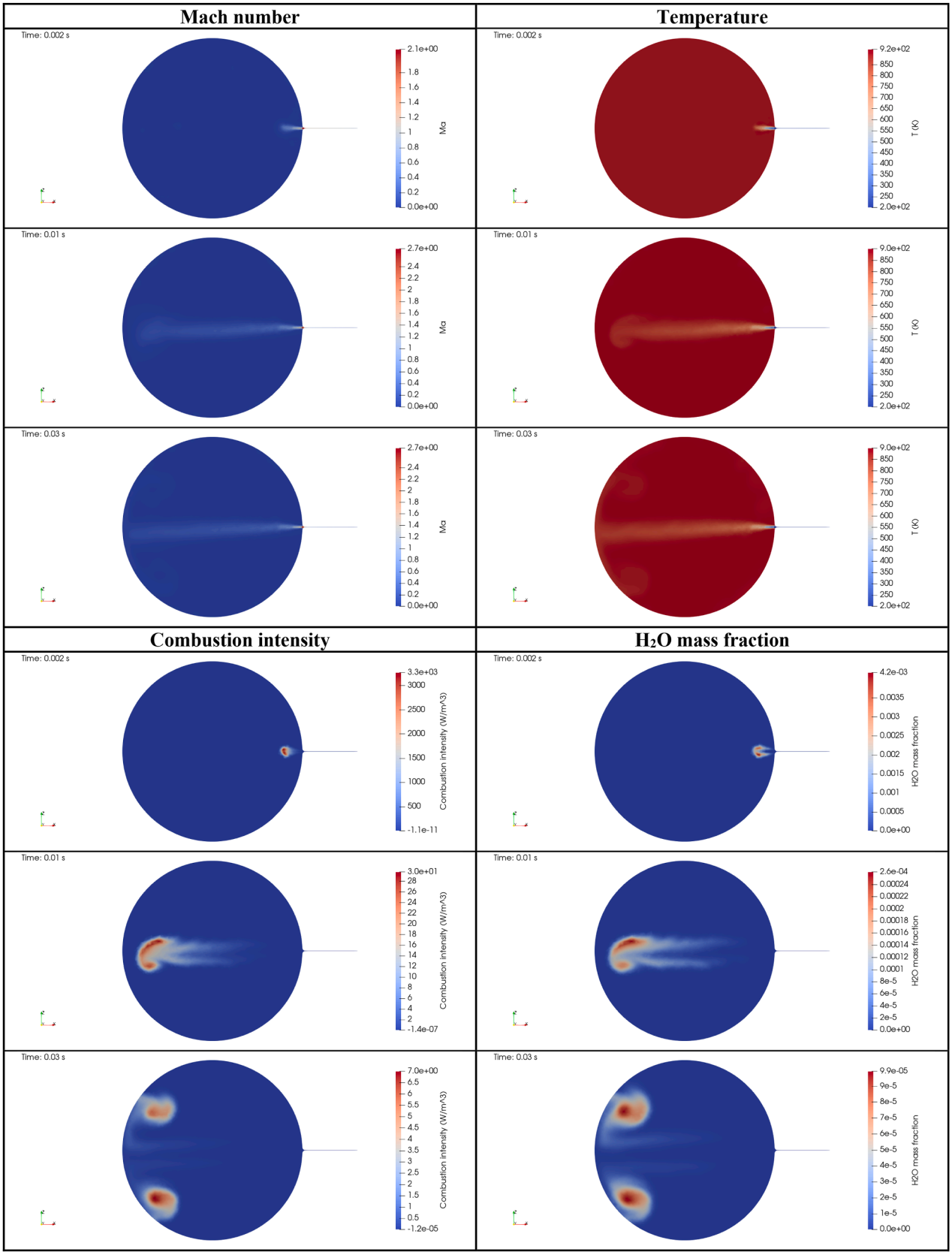

Fig. 5. Fields vs time for Case 2.

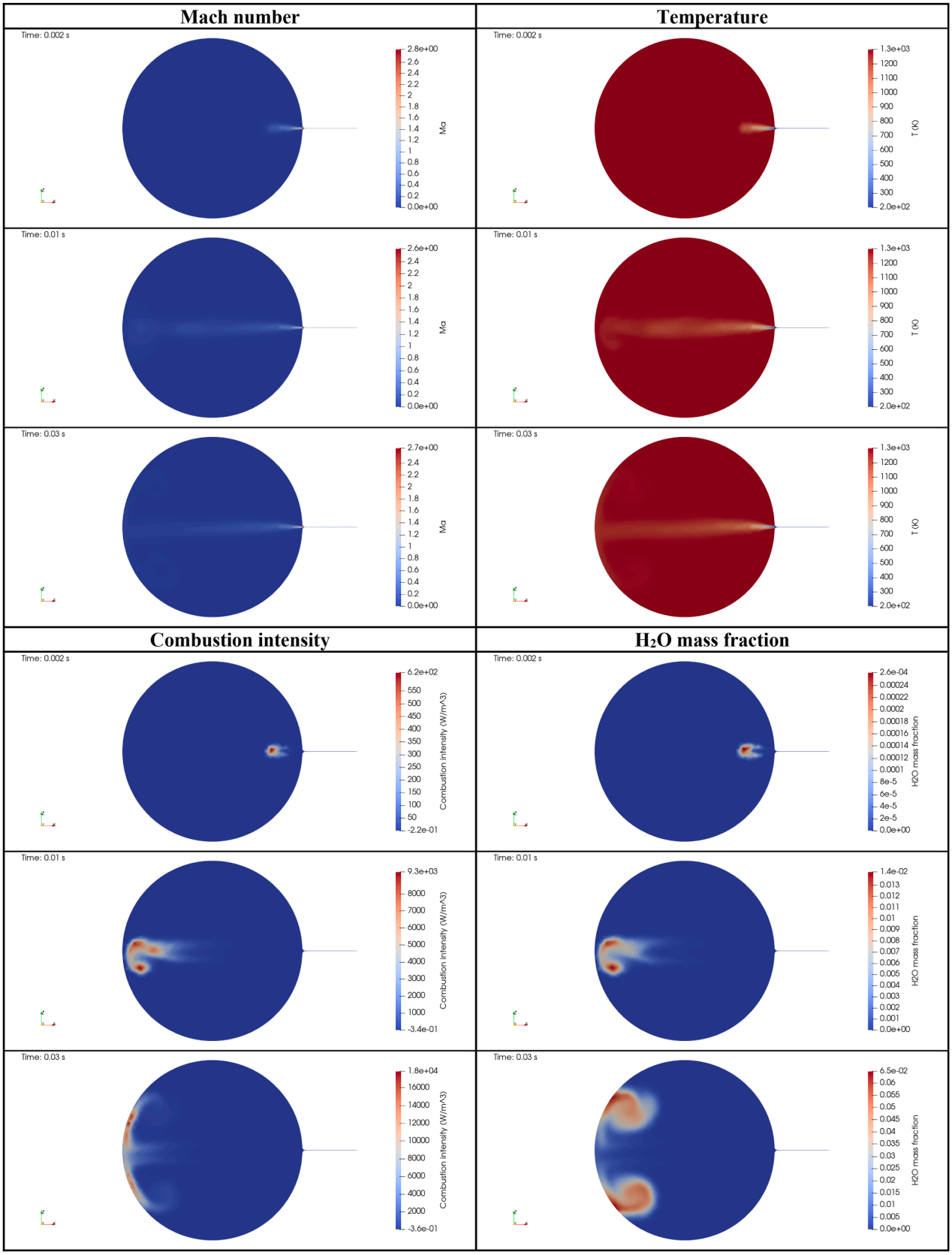

Fig. 6. Fields vs time for Case 3.

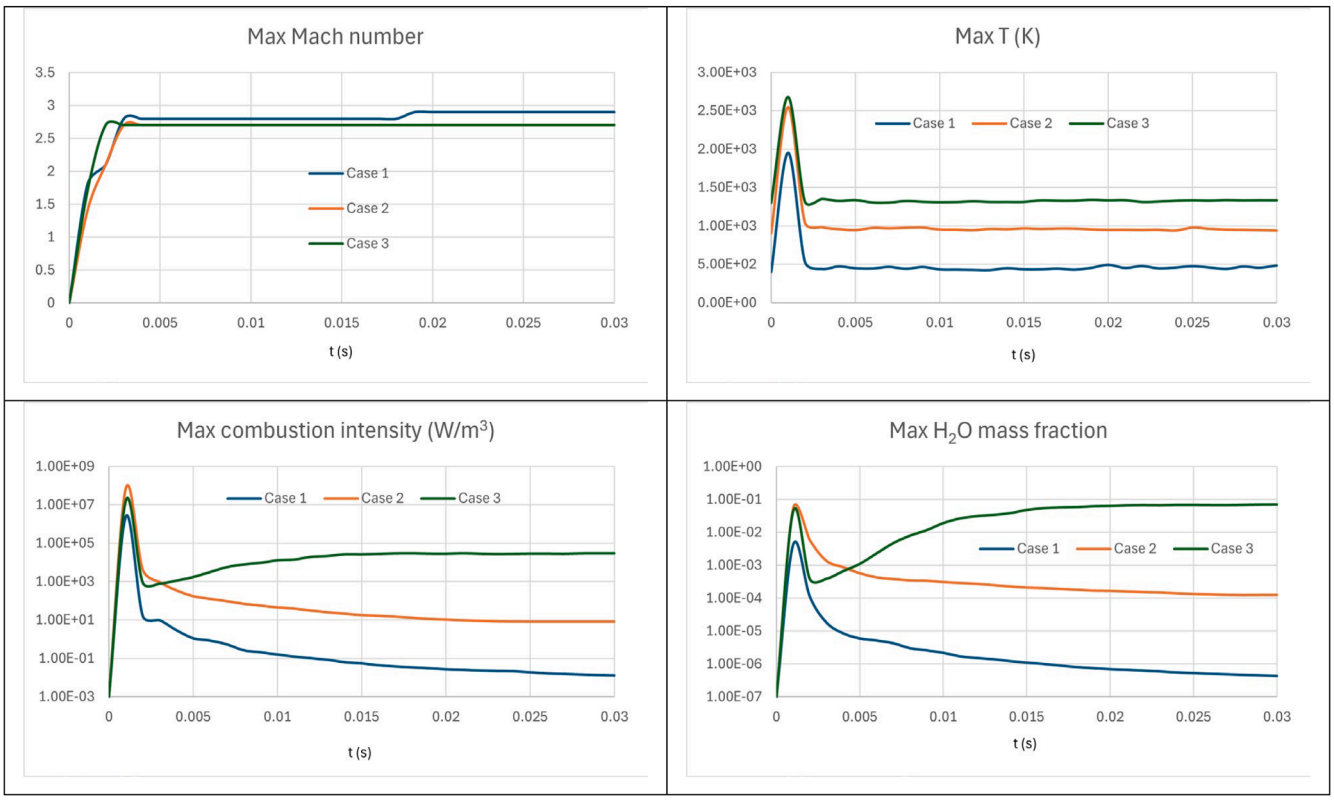

Fig. 7. Comparisons of peak over domain of Mach number, temperature, combustion intensity and water mass fraction versus time.

starts forming at the interface between the jet and the stagnating, low-pressure fuel. Heat production is observed, as well as water formation, at the borders of the jet and especially in counter-rotating vortices (0.01 s and 0.03 s), where air/hydrogen mix and where the speed is lower than in the core of the jet, so that the reactions have more time to occur.

However, the initial temperature (400 K), much lower than the reported ignition one of hydrogen (around 832 K) and the dilution caused by the incoming jet of air below at a temperature below 300 K make the gas mixture to rapidly cool down, which reduces the reaction rates. This effect, combined with the short residence time due to the high speed of the main flow, causes a rapid extinction of the reactions, as can be seen from the drop of combustion intensity and water mass fraction.

Despite the strong initial compressive effect, the resulting intensity of combustion is not sufficient to produce an appreciable impact on temperature in the whole domain.

3.2. Case 2

From a qualitative standpoint, Case 2 transient does not differ from that observed with an initial temperature of 400 K: the incoming jet of air expands supersonically into the vacuum chamber and momentarily ignites the D/T/air mixture by compression, which leads to water and heat production at the forefront of the air stream and in the counter-rotating vortices. Maximum Mach number is lower (2.7) due to the lower expansion ratio of the jet of air, whereas, despite a lower compressive effect, the peak temperature is higher because of its higher initial value. The higher initial temperature leads to a greater heat and water production, because the reaction rate grows with temperature, as stated in Eq. (21), notwithstanding that combustion intensity levels down to about 10 W/m^3.

3.3. Case 3

Mach number and temperature graphs show the same behaviour as for cases 1 and 2. Combustion intensity and water mass fraction, however, start to increase after the initial reduction that is observed previously and tend, at least at this stage, to a steady value. This is due to the fact that because of the higher initial temperature (well above the ignition one), combustion occurs and the flame doesn't extinguish. D/T mixture is so being consumed in the counter-rotating vortices as they progressively enlarge and move rearwards. Combustion intensity reaches a value that is 3 orders of magnitude greater than in Case 2 (about 10^4 instead of 10 W/m^3) and may lead to dust ignition. In this case, it can be concluded that initial temperature is sufficient to ensure a sustained reaction between oxygen and hydrogen isotopes.

4. Conclusions

In this paper, the influence on ignition risk of initial temperature of a D/T mixture in case of a LOVA was investigated by means of numerical CFD simulations caried out on a spherical domain. It was found that at low temperature (400 K), combustion doesn't sustain itself as the compressive effect due to the penetration of a supersonic stream of air only momentarily heats the gas mixture above the ignition temperature, whereas dilution and short residence time strongly reduce mixture temperature and causes extinction. By increasing temperature (900 K), reactions proceed faster and do not seem to stop after 0.03 s, although combustion intensity is low and tends to reduce. At 1300 K, combustion takes place and keeps occurring after 0.03 s.

The overall reaction rate of hydrogen combustion depends on local values of equivalence ratio and temperature, the first factor having to fall into the flammability limits (lower and upper) at that temperature to let combustion occur. In the present study, being the oxidizer (oxygen of air) and fuel (D/T) initially separated (diffusion flame), the composition of the local mixture of reactants covers the whole range of equivalence ratio (from pure fuel inside the vessel at t=0 s to pure oxidiser inside the incoming jet of air) and therefore comprises the flammability one. Therefore, the initial temperature inside the vessel is the factor that

determines whether an ignition of the mixture contained in the vessel ignites or not.

CRediT authorship contribution statement

Jean-François Ciparisse: Investigation. **Danilo Nicola Dongiovanni:** Supervision.

Declaration of competing interest

The authors declare that they have no known competing financial interests or personal relationships that could have appeared to influence the work reported in this paper.

Acknowledgments

This work has been carried out within the framework of the EUROfusion Consortium, funded by the European Union via the Euratom Research and Training Programme (Grant Agreement No 101052200 — EUROfusion). Views and opinions expressed are however those of the author(s) only and do not necessarily reflect those of the European Union or the European Commission. Neither the European Union nor the European Commission can be held responsible for them.

Data availability

No data was used for the research described in the article.

References

[1] A. Denkevits, Hydrogen/dust explosion hazard in ITER: effect of nitrogen dilution on explosion behavior of hydrogen/tungsten dust/air mixtures, Fusion Eng. Des. 85 (7–9) (2010), https://doi.org/10.1016/j.fusengdes.2010.01.009. Issues.
[2] N. Taylor et al. Lessons learnt from ITER safety & licensing for DEMO and future nuclear fusion facilities, Fusion Eng. Des. https://doi.org/10.1016/j.fusengdes.2013.12.030.
[3] M. Povilaitis et al., DEMO BB safety data list (SDL), EUROfusion EFDA_D_2NUYCH 1.1(2022).
[4] Spagnuolo et al., Integration issues on tritium management of the European DEMO breeding blanket and ancillary systems, 10.1016/j.fusengdes.2021.112573.
[5] M. Kuznetsov et al., Experiments for the hydrogen combustion aspects of ITER LOVA scenarios, Fusion Eng. Des. 10.1016/j.fusengdes.2011.01.050.
[6] B.J. Merrill, P. Humrickhouse, R.L. Moore, A recent version of MELCOR for fusion safety applications, Fusion Eng. Des. 85 (2010) 1479–1483.
[7] R. Redlinger, Numerical simulation of hybrid dust/gas explosion experiments in the standard 20-L sphere, Fusion Eng. Des. 100 (2015), https://doi.org/10.1016/j.fusengdes.2015.07.006. Volume.
[8] R. Mével, J. Sabard, J. Lei, N. Chaumeix, Fundamental combustion properties of oxygen enriched hydrogen/air mixtures relevant to safety analysis: experimental and simulation study, Int. J. Hydrog. Energy 41 (16) (2016), https://doi.org/10.1016/j.ijhydene.2016.03.026.
[9] J. Xiao, W. Breitung, M. Kuznetsov, H. Zhang, JR. Travis, R. Redlinger, T. Jordan, GASFLOW-MPI: a new 3-D parallel all-speed CFD code for turbulent dispersion and combustion simulations: part I: models, verification and validation, Int. J. Hydrog. Energy 42 (12) (2017), https://doi.org/10.1016/j.ijhydene.2017.01.215.
[10] M. Povilaitis, J. Jaseliūnaitė, flameFoam: an open source CFD solver for turbulent premixed combustion, Nucl. Eng. Des. 383 (2021), https://doi.org/10.1016/j.nucengdes.2021.111361.
[11] K. Olchewsky et al., Autoignition temperature measurements of hydrogen mixtures, 10th U.S. National Combustion Meeting Organized by the Eastern States Section of the Combustion Institute, conference paper, 2017.
[12] J. Wei, et al., Large eddy simulation of shock-combustion-film interaction at hydrogen injection in a model scramjet combustor, Aerosp. Sci. Technol. 142 (2023) 108683, https://doi.org/10.1016/j.ast.2023.108683.
[13] C.R. Wilke, A viscosity equation for gas mixtures, J. Chem. Phys. 18 (1950) 517–519, https://doi.org/10.1063/1.1747673.
[14] OpenFOAM 12 user guide, 2025 https://doc.cfd.direct/openfoam/user-guide-v12.
[15] F. Nicoud, F. Ducros, Subgrid-scale stress modelling based on the square of the velocity gradient tensor, Flow Turbul. Combust. 62 (1999) 183–200.
[16] G.P. Smith, et al., GRI Mech 3.0 Mechanism, Berkeley University, 2000. http://www.me.berkeley.edu/gri_mech/.
[17] Chemical-Kinetic Mechanisms for Combustion Applications, San Diego Mechanism web page, Mechanical and Aerospace Engineering (Combustion Research),2025 University of California at San Diego, http://combustion.ucsd.edu.
[18] A. Konnov, et al., Yet another kinetic mechanism for hydrogen combustion, Combust. Flame 203 (2019), https://doi.org/10.1016/j.combustflame.2019.01.032.
[19] G. Ya. Gerasimov, et al., Kinetic mechanism of combustion of hydrogen-oxygen mixtures, J. Eng. Phys. Thermophys. 86 (5) (2013). https://link.springer.com/article/10.1007/s10891-013-0919-7.
[20] V.V. Golub, et al., Experimental and numerical investigation of hydrogen gas autoignition, Int. J. Hydrog. Energy 34 (2009), https://doi.org/10.1016/j.ijhydene.2009.01.081.
[21] D. Dongiovanni, et al., DEMO divertor cassette and plasma facing unit in vessel loss-of-coolant accident, Energies 15 (2022) 8879, https://doi.org/10.3390/en15238879. . (Basel).
[22] C. Lu, et al., Numerical study on the effects of rupture disk opening manner on high-pressure hydrogen release and spontaneous ignition, Int. J. Hydrog. Energy (2023), https://doi.org/10.1016/j.ijhydene.2023.11.332.